PHYSICAL REVIEW B **110**, L060405 (2024)

Letter

Competing magnetocrystalline anisotropy and spin-dimension crossover in $Cr_{1+x}Te_2$

Swati Pandey [*] and Soumik Mukhopadhyay
Department of Physics, Indian Institute of Technology Kanpur, Kanpur 208016, India

(Received 28 February 2024; revised 27 May 2024; accepted 19 July 2024; published 7 August 2024)

We present a comprehensive magnetization study of a newly synthesized $Cr_{1+x}Te_2$ (x∼0.15) compound with ferromagnetic order at T_C∼191 K. The results of magnetization and magnetic entropy change suggest a strong interplay of in-plane ferromagnetic spin fluctuations with easy c-axis ferromagnetic critical fluctuations, resulting in competing magnetocrystalline anisotropy. The universal critical scaling analysis further reveals the spin-dimension (n) crossover from Ising ($n = 1$) to XY ($n = 2$) across T_C. This is in contrast to concentrations above $x \geqslant 0.25$ with either Ising ($n = 1$) or Heisenberg ($n = 3$) spin characteristics across the transition. Our study indicates that the magnetic properties of $Cr_{1+x}Te_2$ undergo qualitative change below certain critical concentration.

DOI: 10.1103/PhysRevB.110.L060405

Introduction. Two-dimensional (2D) magnetic layered materials have attracted a lot of attention among researchers due to their potential for novel scientific discoveries as well as industrial applications in spintronics and optoelectronics [1–6]. Accordingly, the synthesis and characterization of new van der Waals (vdW) magnets, viz., $CrXTe_3$ (X = Si, Ge, and Sn) [7–9], Fe_xGeTe_2 (x = 3,4,5) [10,11] chromium trihalides [12,13], and chromium tellurides $Cr_{1+x}Te_2$ [14–26] have accelerated recently. Amongst these 2D vdW ferromagnets, $Cr_{1+x}Te_2$ has triggered a renewed interest due to the high Curie point T_C well beyond room temperature in $Cr_{1.75}Te_2$ [19] and unique magnetic and transport properties [27].

The structural and magnetic properties of $Cr_{1+x}Te_2$ are sensitive to the relative concentrations of Cr and Te [28]. In general, $Cr_{1+x}Te_2$ systems have extra Cr (x) intercalated in the metal-deficient layer along the c axis between alternating stacks of metal-full $CrTe_2$ layers. Systems with higher Cr content ($x \geqslant 0.5$) have relatively higher T_C and in-plane easy magnetization and have been extensively studied for properties such as anomalous Hall effect, topological Hall effect, tunable interlayer exchange coupling, and superstructure twisting [29–32]. For reduced Cr concentration, T_C decreases to 160 K, and magnetic easy ab plane switches to c axis [22]. This occurs due to the variation in lattice parameter "c," which modifies the magnetic anisotropy energy and exchange interaction [33]. However, the lower end of $Cr_{1+x}Te_2$ with $x \leqslant 0.2$ has received less attention. The compound $CrTe_2$ ($x = 0$) without intercalated Cr has rarely been studied in detail due to its difficulty in synthesis. Nonetheless, one study in metastable 1T-$CrTe_2$ reported it to be in-plane ferromagnetic (FM) with T_C∼310 K. First-principles calculations in $CrTe_2$ suggested the possibility of antiferromagnetic (AFM) ground state with compressive strain on the lattice providing a way to tune the competing direct Cr-Cr AFM exchange and the indirect Cr-Te-Cr FM superexchange [34]. Interestingly, 1T-$CrTe_2$ with high T_C and in-plane easy magnetization appears to exhibit the opposite tendency with decreasing Cr concentration and requires further investigation. The paucity of magnetization studies, in particular critical analysis in low Cr-intercalated compounds, restricts our understanding of the nature of magnetic interactions in these systems.

To address concerns related to the ground state in these systems and shed light on the nature of the underlying magnetic correlation, we investigate the critical behavior of the newly synthesized low Cr concentration compound $Cr_{1+x}Te_2$ ($x = 0.15$). In this work, we systematically investigate the nature of magnetic order using magnetization and magnetic entropy change measurements around T_C. We explore the critical exponents around the transition using universal critical scaling analysis, which employs a range of methodologies such as Landau analysis, entropy analysis, and the Kouvel-Fisher (KF) technique to understand the critical behavior of $Cr_{1.15}Te_2$. We argue that the reduced intercalation affects the properties resulting in behavior different from the systems of the same family.

Results. Sample preparation and characterization details are given in the Supplemental Material [35]. Figure 1(a) shows the single crystal x-ray diffraction (XRD) pattern of $Cr_{1.15}Te_2$, with a set of diffraction peaks along (00l), indicating that the crystal's largest natural surface is perpendicular to the c axis and parallel to the ab plane. The Rietveld refined powder XRD pattern is consistent with trigonal structure and confirms the single-phase nature of the system (Fig. S1 [35]). The inset of Fig. 1(a) illustrates its layered structure with extra Cr intercalated in metal-deficient layers along the c axis between alternatively stacked $CrTe_2$ layers. The energy-dispersive x ray (EDX) [Fig. 1(b)] reveals the compositions to be Cr:Te=36.66:63.33. Figure 1(c) presents the magnetic susceptibility $\chi(T)[\equiv M/H]$ measured during zero-field cooling and field cooling in 0.01 T along the c axis and ab plane. On reducing the temperature, the anisotropic behavior

[*]Contact author: swati.910213@gmail.com

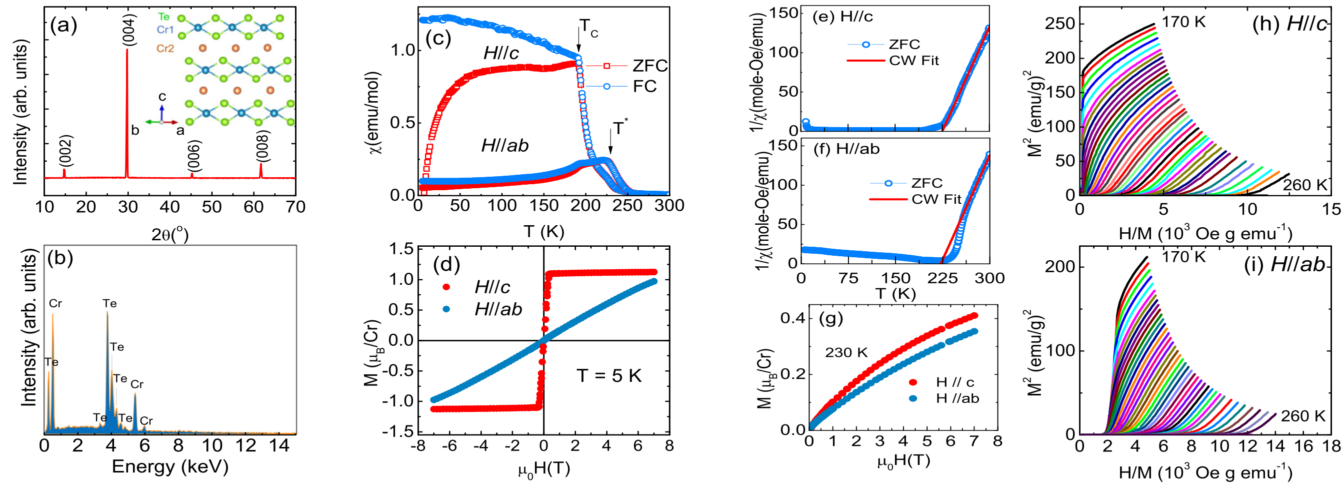

FIG. 1. (a) XRD pattern and crystal structure (inset) of $Cr_{1.15}Te_2$. (b) EDX spectrum of single crystal. $\chi(T)$ along (c) $H \parallel c$ and $H \parallel ab$. (d) $M(H)$ curves along $H \parallel c$ and $H \parallel ab$ at 5 K. $1/\chi$ vs T along (e) $H \parallel c$ and (f) $H \parallel ab$. The red line is the CW fit. (g) $M(H)$ curves for $H \parallel c$ and $H \parallel ab$ at 230 K. Arrott plots at different temperatures across T_C along (h) $H \parallel c$ and (i) $H \parallel ab$.

of magnetization sets in below 260 K as evident from the difference in $\chi(T)$ along $H \parallel c$ and $H \parallel ab$. A clear FM transition along $H \parallel c$ is observed at $T_C{\sim}191$ K which for $H \parallel ab$ is at ∼195 K. Figure 1(d) shows the isothermal magnetization curves $M(H)$ at 5 K, which saturates easily along the $H \parallel c$ direction compared to $H \parallel ab$, indicating the c axis to be the easy magnetization axis. Additionally, a broad humplike feature could be seen above T_C along $H \parallel c$ and $H \parallel ab$ around $T^*{\sim}235$ K. Inspecting its nature along the ab plane, where the feature is prominent, suggests enhanced short-ranged FM spin fluctuations reminiscent of FM order in $1T$-$CrTe_2$ [34,36,37]. The interplay of these in-plane FM spin fluctuations and out-of-plane FM critical fluctuations (highly correlated magnetization fluctuations near a second-order thermodynamical critical point [38]) along different crystallographic directions results in competing anisotropies in our system. This is consistent with the temperature-dependent magnetic anisotropy constant, K_1, which is nonzero above T_C and begins to deviate from perfectly uniaxial behavior (Supplemental Material Fig. S2) [35,39]. A tiny Cr intercalated in a vdW gap enables out-of-plane Cr interactions to overcome substantial in-plane FM spin fluctuations with decreasing temperature, allowing the system to order ferromagnetically at ∼191 K. Whereas, the enhanced 2D in-plane FM spin fluctuations in our case with Cr doping prevent the system from developing a gap in the spin-excitation spectrum, hence impeding ordering at 235 K consistent with the Mermin-Wagner theorem [40,41]. The FM nature of these fluctuations is also evident from the Curie-Weiss (CW) fit in the paramagnetic (PM) region [Figs 1(e) and 1(f)] with positive Weiss temperature ∼225 K [35,42]. Nonetheless, the lack of saturation magnetization with the nonlinear nature of $M(H)$ below T^* [Fig. 1(g)] confirms the short-range nature of the ordering. Moreover, the decreasing $\chi(T)$ [Fig. 1(c)] along the ab plane indicates the in-plane AFM component below T_C in accordance with the reported neutron data, which suggests the canted structure caused by tilting of the FM spins stacked along the c axis towards the ab plane [43–46]. The above results indicate a strong interplay of competing anisotropy and multiple magnetic exchange interactions in the system.

To determine the nature of magnetic interactions, we performed scaling analysis of $Cr_{1.15}Te_2$, for which we have measured isothermal $M(H)$ curves in the temperature range 170–260 K along both directions. Near a second-order phase transition (SOPT), critical exponent analysis is recognized to be a potent method for identifying the relevant microscopic interaction responsible for the transition. According to Banerjee's criterion, around the critical temperature Arrott plots exhibit positive slope for a magnetic SOPT and negative slope for magnetic first-order phase transition (FOPT) [47]. As shown in Figs 1(h) and 1(i), the entire Arrott-plot region has positive slopes, apparently suggesting SOPT. The nonlinear feature in the high-field region of the Arrott plots suggests that critical behavior cannot be described by mean-field theory. Since the Banerjee criterion is not universally applicable, as it is based on a mean-field model, we utilize the iterative method known as the modified Arrott plot (MAP) for the correct estimation of critical exponents β, γ, and δ [35,48–51]. As shown in Fig. 2(a), a set of parallel lines at high fields is achieved using the proper selection of β and γ; here the isotherm at T_C passes through the origin. Figure 2(c) shows the fit of M_S and χ_0^{-1} and the obtained critical exponents are $\beta = 0.346(7)$ and $\gamma = 1.788(6)$. Figure 2(e) represents KF plots $[M_S(dM_S/dT)^{-1}$ and $\chi_0^{-1}(d\chi_0^{-1}/dT)^{-1}$ vs $T]$ to determine the exponents β, γ, and T_C independently [52]. Here, the slopes of the linear fits to the KF plots are $1/\beta$ and $1/\gamma$ while the intercept is T_C. The T_C and critical exponents obtained from KF analysis are $\beta = 0.344(8)$ and $\gamma = 1.779(3)$, which agrees with the MAP analysis. Moreover, exponent $\beta = 6.10(1)$ can be obtained independently by linearly fitting the $M(H)$ curve at T_C on a log-log scale as shown in Fig. 2(g). Furthermore, using the values of β and γ from MAP and KF analyses, the exponent δ calculated from the Widom scaling relation [53], $\delta = 1+\gamma/\beta$, is 6.16(7) and 6.15(9), respectively, close to that obtained from the experiment, confirming the critical exponents to be self-consistent and unambiguous.

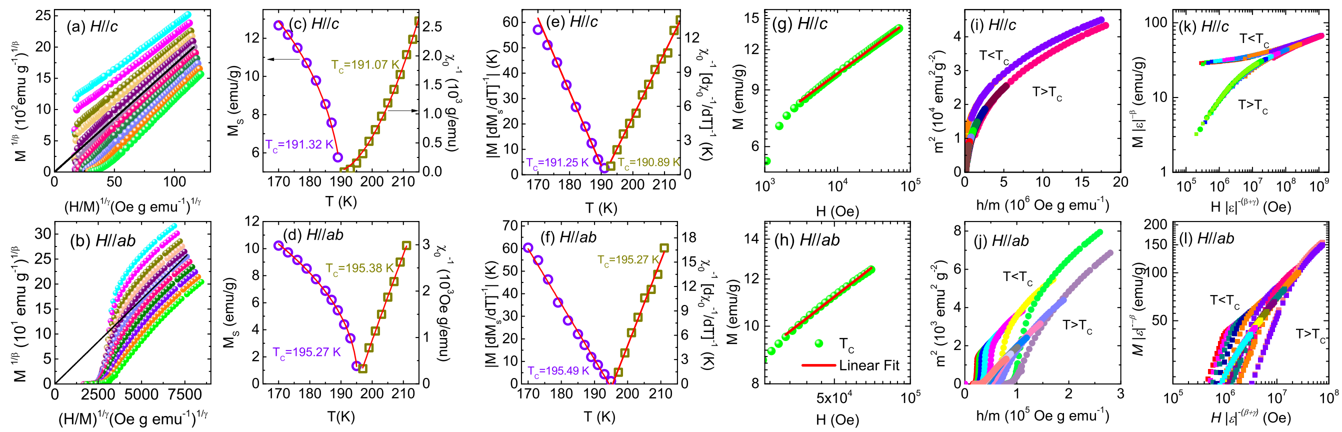

FIG. 2. MAP isotherms for (a) $H \parallel c$ and (b) $H \parallel ab$. M_S (left axis) and $1/\chi_0$ (right axis) vs temperature along (c) $H \parallel c$ and (d) $H \parallel ab$. The red lines are fit to the equation described in text. The KF plots and the corresponding linear fits (red lines) along (e) $H \parallel c$ and (f) $H \parallel ab$. Double logarithmic plot of the $M(H)$ curve at T_C along (g) $H \parallel c$ and (h) $H \parallel ab$. Scaling plots of m^2 vs h/m along (i) $H \parallel c$ and (j) $H \parallel ab$. Scaling plots of $M|\epsilon|^{-\beta}$ vs $H|\epsilon|^{-(\beta+\gamma)}$ in log-log scale along (k) $H \parallel c$ and (l) $H \parallel ab$.

Interestingly, the exponents β, γ, and δ, for the present system (Table I) do not belong to any particular universality class. Rather, it shows the γ and β above and below T_C, respectively, belong to the 2D Ising and 3D *XY* universality classes, suggesting the spin-dimension crossover across T_C. In addition, to confirm the reliability of the critical exponents, a scaling analysis is performed. According to the scaling hypothesis, near the critical region, choosing the critical exponents correctly should result in all initial $M(H)$ curves forming two independent branches, above and below T_C with the $M(H)$ curves satisfying the scaling equation [54]: $m \equiv \epsilon^{-\beta} M(H, \epsilon)$ and $h \equiv H\epsilon^{-(\beta+\gamma)}$, where m and h are the renormalized magnetization and field, respectively. Figure 2(i) shows the scaling plots of m^2 vs h/m below and above T_C, while Fig. 2(k) shows the scaling plots of $M|\epsilon|^{-\beta}$ vs $H|\epsilon|^{-(\beta+\gamma)}$ in log-log scale.

It is important to assess the nature of magnetic correlations along the *ab* plane. Following the procedure similar to $H \parallel c$, the MAP is constructed for $H \parallel ab$ [Fig. 2(b)] resulting in set of parallel lines with the isotherm at T_C passing through the origin. The fitting resulted in the critical exponents $\beta = 0.461(6)$ and $\gamma = 0.947(6)$ and KF plots yield $\beta = 0.455(7)$ and $\gamma = 0.966(1)$, as shown in Figs. 2(d) and 2(f), respectively. Moreover, fitting the initial $M(H)$ curve at T_C on a log-log scale [Fig. 2(h)] provides the exponent $\beta = 3.02(9)$. Using the values of β and γ from MAP and KF analysis, the Widom relation yields $\delta = 3.05(2)$ and $3.12(1)$, respectively, which is close to the experimentally obtained values and suggest the self-consistency of the exponents. The perfect collapse of $M(H)$ curves for fields above 3 T, below and above T_C in two separate curves [Figs. 2(j) and 2(l)] further confirms the reliability of the critical exponents. However, deviation from the scaling behavior of the low-field data indicates the FOPT as discussed further in entropy analysis. Comparing critical exponents along $H \parallel ab$ in Table I indicates long-ranged in-plane magnetic correlations similar to systems above $x > 0.5$ with in-plane anisotropy such as $Cr_{1.66}Te_2$ [55].

Considering the direct correlation between the critical behavior and magnetic entropy change ($-\Delta S_M$), the magnetic entropy calculations are also utilized to obtain the critical exponents and understand the magnetic interactions in

TABLE I. Comparison of the critical exponents of $Cr_{1.15}Te_2$ with theoretical models and related chromium telluride 2D ferromagnets. *d*, spatial dimension; *n*, spin dimensionality; and CI, critical isotherm.

Model/Material	{*d*:*n*}	Technique	β	γ	δ	T_C (K)	Ref.
Mean field		Theory	0.5	1	3		[50]
3D Heisenberg	{3:3}	Theory	0.365	1.386	4.8		[50,69]
3D *XY*	{3:2}	Theory	0.345	1.316	4.81		[50,70]
3D Ising	{3:1}	Theory	0.325	1.24	4.82		[50,70]
2D Ising	{2:1}	Theory	0.125	1.75	15		[71]
$Cr_{1.66}Te_2$		MAP	0.405(1)	1.200(1)	3.96(1)	388	[55]
$Cr_{1.60}Te_2$		MAP	0.387(9)	1.288(5)	4.32(2)	318	[20]
$Cr_{1.24}Te_2$		MAP	0.314(7)	1.83(2)	6.83(7)	230.76(9)	[14]
$Cr_{1.15}Te_2$ $H \parallel c$		MAP	0.346(7)	1.788(6)	6.16(7)	191.32	This work
		KF	0.344(8)	1.779(3)	6.15(9)	191.25	
		CI			6.10(1)		
$H \parallel ab$		MAP	0.461(6)	0.947(6)	3.05(2)	195.27	This work
		KF	0.455(7)	0.966(1)	3.12(1)	195.49	
		CI			3.02(9)		

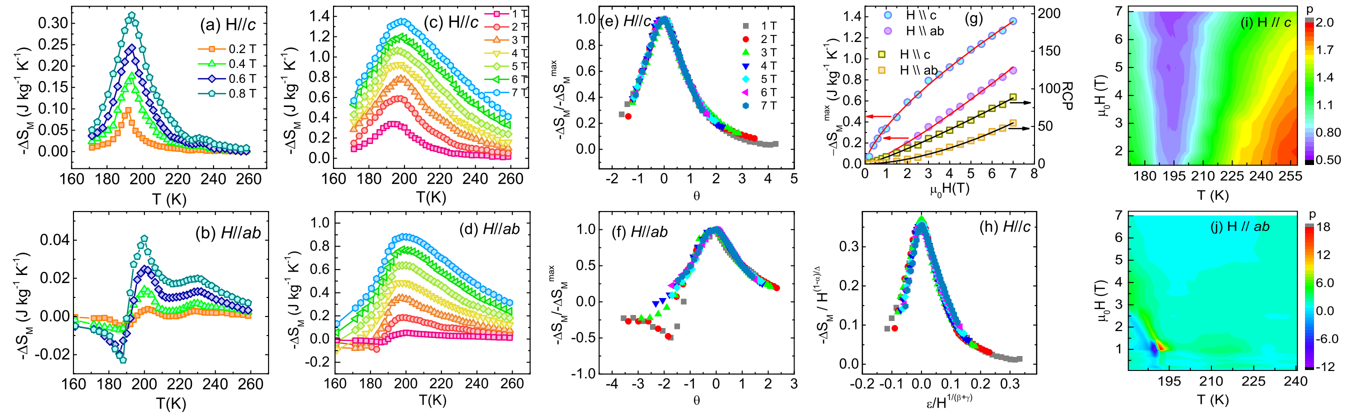

FIG. 3. $-\Delta S_M$ vs temperature up to 0.8 T along (a) $H \parallel c$ and (b) $H \parallel ab$ and from 1–7 T along (c) $H \parallel c$ and (d) $H \parallel ab$. $-\Delta S_M/-\Delta S_M^{\max}$ vs θ along (e) $H \parallel c$ and (f) $H \parallel ab$. (g) $-\Delta S_M^{\max}$ (left axis) and RCP (right axis) vs H. Black and red lines are power-law fits. (h) Scaling plots as described in text for $H \parallel c$. Field temperature dependence of p for (i) $H \parallel c$, and (j) $H \parallel ab$.

$Cr_{1.15}Te_2$. This approach provides insight into the order of transition and yields model-independent critical exponents, and hence is considered more reliable. The ΔS_M curves are obtained from the $M(H)$ curves using Maxwell's relation [56–58]:

$$\Delta S_M(T, \Delta H) = \int_{H_i}^{H_f} [\partial M(T, H)/\partial T]_H dH, \tag{1}$$

where H_i and H_f are the initial and final fields, respectively. A maximum around T_C in $(-\Delta S_M)$ for $H \parallel c$ [Fig. 3(a)], shows the conventional magnetic entropy change [positive $(-\Delta S_M)$], consistent with the PM to FM transition [59,60]. On the other hand, for $H \parallel ab$ [Fig. 3(b)] the maximum corresponding to conventional magnetic entropy change at T_C shows a crossover to inverse magnetic entropy change [negative $(-\Delta S_M)$], consistent with the AFM transition, complying with the presence of an in-plane AFM component below T_C [59,60]. The FM spin fluctuations at T^* evident as a small hump above T_C at lower fields along both the directions is seen to be suppressed above 1 T. Nevertheless, the conventional entropy change at T^* indicates the FM nature of the fluctuations. In Figs. 3(c) and 3(d), we plot $(-\Delta S_M)$ as a function of temperature at constant magnetic fields up to 7 T along $H \parallel c$ and $H \parallel ab$, respectively. The maximum value of magnetic entropy change $(-\Delta S_M^{\max})$ at 7 T reaches 1.34 J/kg K along $H \parallel c$, which is roughly 34% greater than that of 0.89 J/kg K along $H \parallel ab$.

To determine the nature of the phase transition, we plotted normalized magnetic entropy curves $(-\Delta S_M/-\Delta S_M^{\max})$ against the rescaled temperature (θ) as shown in Figs. 3(e) and 3(f), where θ is given by

$$\theta = \begin{cases} -(T - T_{\text{peak}})/(T_{r1} - T_{\text{peak}}), & T \leqslant T_{\text{peak}} \\ (T - T_{\text{peak}})/(T_{r2} - T_{\text{peak}}), & T > T_{\text{peak}} \end{cases}, \tag{2}$$

where T_{r1} and T_{r2} are two reference temperatures corresponding to $(-\Delta S_M^{\max})/2$ [61]. Interestingly, the curves at lower fields for $H \parallel ab$ [Fig. 3(f)] do not collapse onto a single curve, suggesting FOPT. Nevertheless, the curves above 3 T do scale perfectly and suggest the field-induced SOPT.

Furthermore, the $-\Delta S_M$ curves could be utilized to obtain the critical exponents and to establish the universality of the exponents obtained from the magnetic critical scaling analysis. The plots of $-\Delta S_M^{\max}$ as a function of field for $H \parallel c$ and $H \parallel ab$ are shown in Fig. 3(g) which follows the power law $|-\Delta S_M| \propto H^p$. The exponent $p = 0.69$ for $H \parallel c$ is in line with the expected value of 0.66 near a SOPT [62], while the exponent $p = 1.22$ for $H \parallel ab$ indicates a discrepancy with SOPT. Figure 3(g) also shows the field dependence of relative cooling power (RCP) $\propto H^q$, where RCP $= \Delta S_M^{\max} \times \delta H^{\text{FWHM}}$, δH^{FWHM} being full width at half maximum of the $-\Delta S_M$-T curve. The value of RCP at 7 T is 89.18 and 54.95 J/kg for $H \parallel c$ and $H \parallel ab$, respectively. Using the value of the exponents p and q, we determine the critical exponents from the following relations: $p = 1 + [(\beta - 1)/(\beta + \gamma)]$ and $q = 1 + (1/\delta)$.

The obtained critical exponents for $H \parallel c$ (Table I) are consistent with the magnetization analysis results where β and γ belong to the 3D XY and 2D Ising universality classes, indicating spin-dimension crossing across T_C. Furthermore, to validate the reliability of the obtained exponents we utilize the scaling equation of state [63,64], $\Delta S_M = H^{(1-\alpha)/\Delta} S(\epsilon/H^{1/\Delta})$, where $\Delta = \beta\delta$, $\alpha = 2 - 2\beta - \gamma$, and S is the scaling function and Fig. 3(h) describes the universal scaling based on this equation. The collapse onto the universal curve confirms the reliability of the critical exponents obtained by the magnetic entropy change.

Furthermore, we exploit the quantitative criterion based on magnetic entropy data as proposed by Law *et al.* to determine the order of the magnetic phase transition, using the temperature- and field-dependent exponent p [65]. The local value of the exponent p at each temperature and magnetic field can be calculated using $p(H, T) = d(\ln|\Delta S|)/d(\ln H)$. Figures 3(i) and 3(j) show the 2D plots of the temperature and field dependence of p for $H \parallel c$ and $H \parallel ab$, respectively. For $H \parallel c$ [Fig. 3(i)], the variation of p clearly suggests the SOPT, where the value of p tends to 1 and 2 below and above the transition temperature, respectively, with a minimum value of 2/3 at T_C. However, for $H \parallel ab$, the overshoot of $p > 2$ is clearly observed albeit within a limited region in the (H,T)

space which suggests the existence of the FOPT. The FOPT in our case is similar to $Cr_{1.33}Te_2$ and can be attributed to spin-lattice coupling assisted transition [22]. Furthermore, the suppression of FOPT into a SOPT in low magnetic field suggests the weak first-order nature of the transition and a tricrtical phenomenon.

Discussion. In order to compare the present system with other $Cr_{1+x}Te_2$ compounds and theoretical models, we have listed the critical exponents in Table I. As can be seen from the table, $Cr_{1.15}Te_2$ cannot be categorized into any of the conventional universality classes. This scenario may arise due to the presence of competing interactions that cannot be adequately captured by a single model. The different exponents for each system result from the strong dependency of the magnetic properties on the Cr concentration. We note that the magnetic correlations evolve from the 3D Heisenberg ($n = 3$) model for higher Cr content in $Cr_{1.60}Te_2$ to the 3D Ising ($n = 1$) model with intermediate Cr content in $Cr_{1.24}Te_2$. The *XY* ($n = 2$) character of critical fluctuations in our case suggests the change in dimensionality of exchange interaction and can be attributed to the extremely low Cr content in the vdW gaps and indicates the weakening of interlayer coupling with negligible correlations between the adjacent *ab* plane. The increased value of γ further suggests a reduced dimension of critical fluctuations [14,66,67] and strongly supports the spins lying along the plane, as also evident from our magnetization results with in-plane FM spin fluctuations competing with easy *c*-axis FM critical fluctuations. In our case, magnetocrystalline anisotropy competition causes a temperature-induced spin-dimension crossover from Ising to *XY* across T_C within the $Cr_{1+x}Te_2$ family, which is rarely studied using critical behavior. Nevertheless, the presence of non-negligible intercalated Cr content can cause the lattice to be 3D in nature. The resulting 3D *XY* universality class has only been reported for a few magnetic systems [68]. Further, the range and dimensionality of the magnetic interactions can also be determined by the dependence of the universality class on the exchange interaction $J(r)$. Based on the renormalization group (RG) theory, the magnetic interaction decays as $J(r) \sim r^{-(d+\sigma)}$, where r is the distance and σ is the range of the exchange interaction. The constant σ can be obtained using the following expression [71,72]:

$$\gamma = 1 + \frac{4}{d}\frac{n+2}{n+8}\Delta\sigma + 8\frac{(n+2)(n-4)}{d^2(n+8)^2} \times \left[1 + \frac{2G\left(\frac{d}{2}\right)(7n+20)}{(n-4)(n-8)}\right]\Delta\sigma^2, \tag{3}$$

where $\Delta\sigma = [\sigma - (d/2)]$, $G(d/2) = 3 - [(1/4)(d/2)^2]$. In general, for homogeneous systems, the range of spin interaction is long or short depending on $\sigma < 2$ or $\sigma > 2$, and the mean-field model is satisfied when $\sigma \leqslant 3/2$. Here, for the parameters $\{d{:}n\}$, σ is varied to obtain a value of γ close to the experimentally obtained value. Following Eq. (3), for our experimental value of γ we have obtained $\sigma = 1.61$ with $d{:}n = 2{:}1$ for $H \parallel c$, and $\sigma = 1.41$ with $d{:}n = 3{:}3$ for $H \parallel ab$ indicating that the spin-spin interactions are long ranged in nature. The value of σ for $H \parallel c$ is greater than that of $H \parallel ab$, again indicating the reduction in the range of spin interactions along the c axis and strengthening of the in-plane interactions. The exchange decays with distance as $J(r) \sim r^{-3.61}$ for $H \parallel c$ and $J(r) \sim r^{-4.41}$ for $H \parallel ab$. Importantly, this indicates that the magnetic coupling's short-range character switches to a long-range one as x decreases. $Cr_{1.24}Te_2$ [14] is at the boundary, with both short-and long-range order, suggesting that it is the optimal concentration below which the magnetic trend shifts as a result of competing magnetic exchange and magnetocrystalline anisotropy. Clearly, the exponents for $H \parallel c$ cannot be described by a single universality class and are located between the theoretical 2D Ising model and the 3D *XY* model. It is generally accepted that the critical exponents on the two sides of a SOPT should be identical according to the general RG argument. If the correlation functions satisfy the same RG equation above and below T_C, or in other words, the renormalization properties of a theory are identical in its symmetric and spontaneously broken phases, it follows that the critical exponents are identical in both phases. However, long ago, Nelson [73] proposed a counterexample based on the 3D Heisenberg-*XY* model with either a cubic or hexagonal anisotropy. Very recently, a generic mechanism was proposed [74] to obtain different critical exponents above and below T_C, which relies on the possibility of explicitly breaking a continuous symmetry down to a discrete one by terms that are irrelevant in the RG sense. Interestingly, a similar difference of critical exponents has also been observed experimentally for noncollinear systems [75–80]. We hope that the results of the critical analysis presented here will initiate more theoretical studies in the future.

Conclusions. The magnetization and magnetic entropy change in $Cr_{1.15}Te_2$ single crystal are systematically investigated. We observe a clear transition from the paramagnetic to ferromagnetic phase at T_C with ferromagnetic instability at higher temperatures. The extracted critical exponents suggest a peculiar phase transition marked by the distinct universality class of the 3D *XY* model and the 2D Ising model on either side of T_C. The change in nature of the spin-spin interaction Hamiltonian across the critical temperature suggests a nontrivial phase transition beyond the Landau-Ginsburg paradigm associated with spontaneous symmetry breaking or the Wilson-Fisher's RG approach on critical behavior.

Acknowledgments. S.P. acknowledges IIT Kanpur, India for financial support. S.M. thanks Department of Science and Technology (DST), Government of India for financial support.

[1] K. S. Novoselov, A. Mishchenko, A. Carvalho, and A. H. Castro Neto, Science **353**, 6298 (2016).

[2] B. Huang, G. Clark, E. Navarro-Moratalla, D. R. Klein, R. Cheng, K. L. Seyler, D. Zhong, E. Schmidgall, M. A. McGuire, D. H. Cobden, W. Yao, D. Xiao, P. Jarillo-Herrero, and X. Xu, Nature (London) **546**, 270 (2017).

[3] D. L. Cortie, G. L. Causer, K. C. Rule, H. Fritzsche, W. Kreuzpaintner, and F. Klose, Adv. Funct. Mater. **30**, 1901414 (2019).

[4] G. Hu and B. Xiang, Nanoscale Res. Lett. **15**, 226 (2020).

[5] H. Kurebayashi, J. H. Garcia, S. Khan, J. Sinova, and S. Roche, Nat. Rev. Phys. **4**, 150 (2022).

[6] G. R. Bhimanapati *et al.*, ACS Nano **9**, 11509 (2015).
[7] N. Sivadas, M. W. Daniels, R. H. Swendsen, S. Okamoto, and D. Xiao, Phys. Rev. B **91**, 235425 (2015).
[8] H. L. Zhuang, Y. Xie, P. R. C. Kent, and P. Ganesh, Phys. Rev. B **92**, 035407 (2015).
[9] L. D. Casto, A. J. Clune, M. O. Yokosuk, J. L. Musfeldt, T. J. Williams, H. L. Zhuang, M.-W. Lin, K. Xiao, R. G. Hennig, B. C. Sales, J.-Q. Yan, and D. Mandrus, APL Mater. **3**, 041515 (2015).
[10] A. F. May, S. Calder, C. Cantoni, H. Cao, and M. A. McGuire, Phys. Rev. B **93**, 014411 (2016).
[11] S. Mondal, N. Khan, S. M. Mishra, B. Satpati, and P. Mandal, Phys. Rev. B **104**, 094405 (2021).
[12] O. Besbes, S. Nikolaev, N. Meskini, and I. Solovyev, Phys. Rev. B **99**, 104432 (2019).
[13] C. Xu, J. Feng, S. Prokhorenko, Y. Nahas, H. Xiang, and L. Bellaiche, Phys. Rev. B **101**, 060404(R) (2020).
[14] Y. Liu and C. Petrovic, Phys. Rev. B **96**, 134410 (2017).
[15] Y. Wang, J. Yan, J. Li, S. Wang, M. Song, J. Song, Z. Li, K. Chen, Y. Qin, L. Ling, H. Du, L. Cao, X. Luo, Y. Xiong, and Y. Sun, Phys. Rev. B **100**, 024434 (2019).
[16] D. Zhao, L. Zhang, I. A. Malik, M. Liao, W. Cui, X. Cai, C. Zhang, L. Li, X. Hu, D. Zhang *et al.*, Nano Res. **11**, 3116 (2018).
[17] G. Cao, Q. Zhang, M. Frontzek, W. Xie, D. Gong, G. E. Sterbinsky, and R. Jin, Phys. Rev. Mater. **3**, 125001 (2019).
[18] Y. Liu, M. Abeykoon, E. Stavitski, K. Attenkofer, and C. Petrovic, Phys. Rev. B **100**, 245114 (2019).
[19] J. Liu, B. Ding, J. Liang, X. Li, Y. Yao, and W. Wang, ACS Nano **16**, 13911 (2022).
[20] L.-Z. Zhang, A.-L. Zhang, X.-D. He, X.-W. Ben, Q.-L. Xiao, W.-L. Lu, F. Chen, Z. Feng, S. Cao, J. Zhang and J.-Y. Ge, Phys. Rev. B **101**, 214413 (2020).
[21] A. Mohamed, Y. Fujisawa, T. Onishi, M. Pardo-Almanza, M. Couillard, K. Harada, T. Takeuchi, and Y. Okada, Phys. Rev. B **106**, 155112 (2022).
[22] Z. Z. Jiang, X. Liang, X. Luo, J. J. Gao, W. Wang, T. Y. Wang, X. C. Yang, X. L. Wang, L. Zhang, Y. Sun, P. Tong, J. F. Hu, W. H. Song, W. J. Lu, and Y. P. Sun, Phys. Rev. B **106**, 094407 (2022).
[23] Y. Wang, S. Kajihara, H. Matsuoka, B. K. Saika, K. Yamagami, Y. Takeda, H. Wadati, K. Ishizaka, Y. Iwasa, and M. Nakano, Nano Lett. **22**, 9964 (2022).
[24] Y. Fujisawa, M. Pardo-Almanza, C.-H. Hsu, A. Mohamed, K. Yamagami, A. Krishnadas, G. Chang, F.-C. Chuang, K. H. Khoo, J. Zang *et al.*, Adv. Mater. **35**, 2207121 (2023).
[25] Z. Shu, H. Wang, N. H. Jo, C. Jozwiak, A. Bostwick, E. Rotenberg, W. Xie, and T. Kong, Phys. Rev. Mater. **7**, 044406 (2023).
[26] A. Wang, A. Rahman, Z. Du, J. Zhao, F. Meng, W. Liu, J. Fan, C. Ma, M. Ge, L. Pi, L. Zhang, and Y. Zhang, Phys. Rev. B **108**, 094429 (2023).
[27] R. Saha, H. L. Meyerheim, B. Gobel, B. K. Hazra, H. Deniz, K. Mohseni, V. Antonov, A. Ernst, D. Knyazev, A. Bedoya-Pinto, I. Mertig, and S. S. P. Parkin, Nat. Commun. **13**, 3965 (2022).
[28] W. Bensch, O. Helmer, and C. Nather, Mater. Res. Bull. **32**, 305 (1997).
[29] S. Purwar, A. Low, A. Bose, A. Narayan, and S. Thirupathaiah, Phys. Rev. Mater. **7**, 094204 (2023).
[30] X. Zhang *et al.*, Adv. Funct. Mater. **32**, 2202977 (2022).
[31] X. Y. Wen, Z. Liu, Y. Zhang, C. Xia, B. Zhai, X. Zhang, G. Zhai, C. Shen, P. He, R. Cheng, L. Yin, Y. Yao, M. Sendeku, Z. Wang, X. Ye, C. Liu, C. Jiang, C. Shan, Y. Long, and J. He, Nano Lett. **20**, 3130 (2020).
[32] A. L. Coughlin, D. Xie, X. Zhan, Y. Yao, L. Deng, H. Hewa-Walpitage, T. Bontke, C. W. Chu, Y. Li, J. Wang, H. A. Fertig, and S. Zhang, Nano Lett. **21**, 9517 (2021).
[33] I. H. Lee *et al.*, ACS Appl. Nano Mater. **4**, 4810 (2021).
[34] H. Y. Lv, W. J. Lu, D. F. Shao, Y. Liu, and Y. P. Sun, Phys. Rev. B **92**, 214419 (2015).
[35] See Supplemental Material at http://link.aps.org/supplemental/10.1103/PhysRevB.110.L060405 for experimental details, sample characterization, description of anisotropy, Curie-Weiss temperature, and the modified Arrott plot.
[36] D. C. Freitas, R. Weht, A. Sulpice, G. Remenyi, P. Strobel, F. Gay, J. Marcus, and M. Nunez-Regueiro, J. Phys.: Condens. Matter **27**, 176002 (2015).
[37] K. Shimada, T. Saitoh, H. Namatame, A. Fujimori, S. Ishida, S. Asano, M. Matoba, and S. Anzai, Phys. Rev. B **53**, 7673 (1996).
[38] C. Jin, Z. Tao, K. Kang, K. Watanabe, T. Taniguchi, K. F. Mak, and J. Shan, Nat. Mater. **19**, 1290 (2020).
[39] W. Sucksmith and J. E. Thompson, Proc. Roy. Soc. A **225**, 362 (1954).
[40] N. D. Mermin and H. Wagner, Phys. Rev. Lett. **17**, 1133 (1966).
[41] C. Gong, L. Li, Z. Li, H. Ji, A. Stern, Y. Xia, T. Cao, W. Bao, C. Wang, Y. Wang, Z. Q. Qiu, R. J. Cava, S. G. Louie, J. Xia, and X. Zhang, Nature (London) **546**, 265 (2017).
[42] J. Blawat, M. Marshall, J. Singleton, E. Feng, H. Cao, W. Xie, and R. Jin, Adv. Quantum Technol. **5**, 2200012 (2022).
[43] A. F. Andresen, Acta Chem. Scand. **17**, 1335 (1963).
[44] A. F. Andresen, Acta Chem. Scand. **24**, 3495 (1970).
[45] T. Hamasaki, T. Hashimoto, Y. Yamaguchi, and H. Watanabe, Solid State Commun. **16**, 895 (1975).
[46] W. J. Takei, D. E. Cox, and G. Shirane, J. Appl. Phys. **37**, 973 (1966).
[47] B. K. Banerjee, Phys. Lett. **12**, 16 (1964).
[48] A. Arrott and J. E. Noakes, Phys. Rev. Lett. **19**, 786 (1967).
[49] M. E. Fisher, Rep. Prog. Phys. **31**, 418 (1968).
[50] H. E. Stanley, Rev. Mod. Phys. **71**, S358 (1999).
[51] A. K. Pramanik and A. Banerjee, Phys. Rev. B **79**, 214426 (2009).
[52] J. S. Kouvel and M. E. Fisher, Phys. Rev. **136**, A1626 (1964).
[53] A. Hankey and H. E. Stanley, Phys. Rev. B **6**, 3515 (1972).
[54] S. N. Kaul, J. Magn. Magn. Mater. **53**, 5 (1985).
[55] L.-Z. Zhang, Q.-L. Xiao, F. Chen, Z. Feng, S. Cao, J. Zhang, and J.-Y. Ge, J. Magn. Magn. Mater. **546**, 168770 (2022).
[56] H. E. Stanley, *Phase Transitions and Critical Phenomena* (Clarendon Press, Oxford, 1971), Vol. 7, p. 175.
[57] A. K. Mishra and V. Ganesan, Phys. Rev. B **100**, 125113 (2019).
[58] K. A. Gschneidner, V. K. Pecharsky, and A. O. Tsokol, Rep. Prog. Phys. **68**, 1479 (2005).
[59] R. Rawat and I. Das, Phys. Rev. B **64**, 052407 (2001).
[60] S. Pandey, V. Siruguri, and R. Rawat, J. Phys.: Condens. Matter **32**, 035807 (2019).
[61] C. M. Bonilla, J. Herrero-Albillos, F. Bartolome, L. M. Garcia, M. Parra-Borderias, and V. Franco, Phys. Rev. B **81**, 224424 (2010).
[62] V. Franco, J. S. Blazquez, and A. Conde, Appl. Phys. Lett. **89**, 222512 (2006).
[63] R. B. Griffiths, Phys. Rev. **158**, 176 (1967).

[64] V. Franco, A. Conde, J. M. Romero-Enrique, and J. S. Blazquez, J. Phys.: Condens. Matter **20**, 285207 (2008).
[65] J. Y. Law, V. Franco, L. M. Moreno-Ramirez, A. Conde, D. Y. Karpenkov, I. Radulov, K. P. Skokov, and O. Gutfleisch, Nat. Commun. **9**, 2680 (2018).
[66] W. Liu, Y. Wang, J. Fan, L. Pi, M. Ge, L. Zhang, and Y. Zhang, Phys. Rev. B **100**, 104403 (2019).
[67] W. Liu, Y. Dai, Y.-E. Yang, J. Fan, L. Pi, L. Zhang, and Y. Zhang, Phys. Rev. B **98**, 214420 (2018).
[68] A. Oleaga, A. Salazar, D. Prabhakaran, J.-G. Cheng, and J.-S. Zhou, Phys. Rev. B **85**, 184425 (2012).
[69] M. Campostrini, M. Hasenbusch, A. Pelissetto, P. Rossi, and E. Vicari, Phys. Rev. B **65**, 144520 (2002).
[70] J. C. Le Guillou and J. Zinn-Justin, Phys. Rev. B **21**, 3976 (1980).
[71] S. F. Fischer, S. N. Kaul, and H. Kronmuller, Phys. Rev. B **65**, 064443 (2002).
[72] M. E. Fisher, S.-K. Ma, and B. Nickel, Phys. Rev. Lett. **29**, 917 (1972).
[73] D. R. Nelson, Phys. Rev. B **13**, 2222 (1976).
[74] F. Leonard and B. Delamotte, Phys. Rev. Lett. **115**, 200601 (2015).
[75] F. Meng, W. Liu, A. Rahman, J. Zhang, J. Fan, C. Ma, M. Ge, T. Yao, L. Pi, L. Zhang, and Y. Zhang, Phys. Rev. B **107**, 144425 (2023).
[76] J. Yan, X. Luo, F. C. Chen, J. J. Gao, Z. Z. Jiang, G. C. Zhao, Y. Sun, H. Y. Lv, S. J. Tian, Q. W. Yin, H. C. Lei, W. J. Lu, P. Tong, W. H. Song, X. B. Zhu, and Y. P. Sun, Phys. Rev. B **100**, 094402 (2019).
[77] G. T. Lin, X. Luo, F. C. Chen, J. Yan, J. J. Gao, Y. Sun, W. Tong, P. Tong, W. J. Lu, Z. G. Sheng, W. H. Song, X. B. Zhu, and Y. P. Sun, Appl. Phys. Lett. **112**, 072405 (2018).
[78] L. Zhang, H. Han, M. Ge, H. Du, C. Jin, W. Wei, J. Fan, C. Zhang, L. Pi, and Y. Zhang, Sci. Rep. **6**, 22397 (2016).
[79] X. Yang, J. Pan, X. He, S. Liu, H. Jia, L. Cao, and M. Yang, New J. Phys. **24**, 093001 (2022).
[80] H. C. Chauhan, B. Kumar, A. Tiwari, J. K. Tiwari, and S. Ghosh, Phys. Rev. Lett. **128**, 015703 (2022).